Electronic Supplementary Information (ESI)

Adding value to terpenes: Copper-catalyzed oxidation of α-pinene in water under micellar conditions

Gilvan A. Correia[1], Chris H. J. Franco[1], Marina V. Kirillova[1], Fabrice Gallou[2] and Alexander M. Kirillov[1*]

[1]*MINDlab: Molecular Design & Innovation Laboratory, Centro de Química Estrutural, Institute of Molecular Sciences, Departamento de Engenharia Química, Instituto Superior Técnico, Universidade de Lisboa, Av. Rovisco Pais, 1049-001, Lisboa, Portugal.*

[2]*Chemical & Analytical Development, Novartis Pharma AG, 4056, Basel, Switzerland.*

Contents

Section 1 – Synthesis and Characterization of compounds 1, 2, and 3

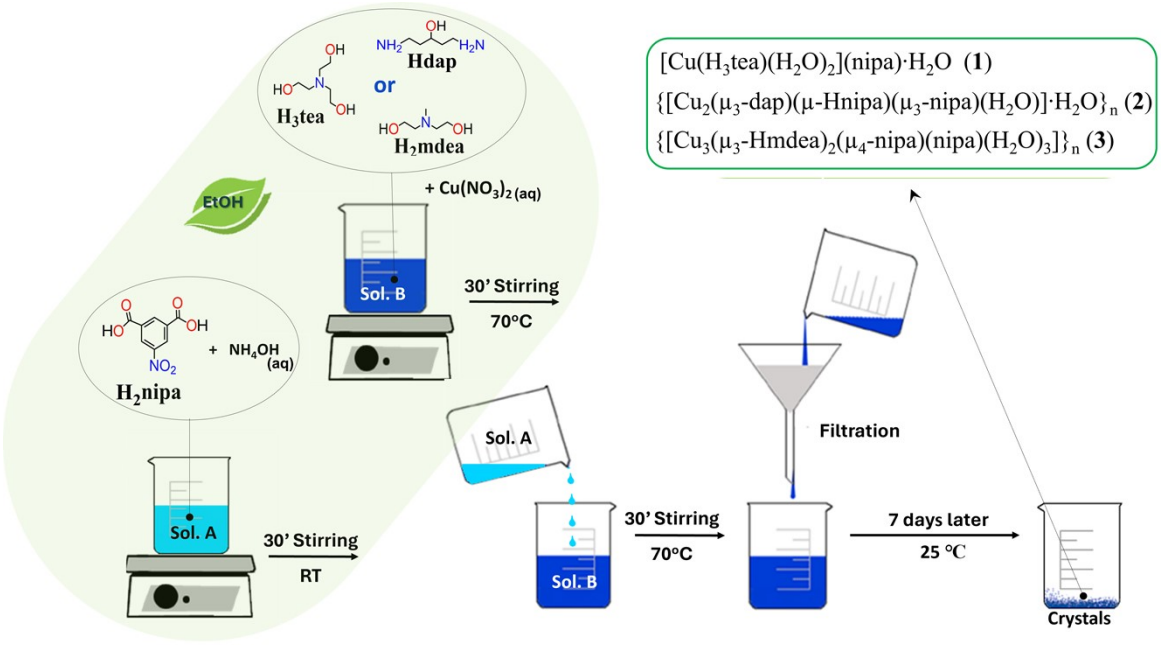

Figure S1. Schematic representation of the synthesis of compounds **1**, **2**, and **3**.

Materials and methods. All chemicals and solvents were acquired commercially and utilized without any prior preparation. Elemental analyses (C, H, N) were carried out on a PerkinElmer PE 2400 Series II analyzer (Laboratory of Analyses, IST). The infrared spectra were recorded in the range of 4000–600 cm^{-1} on an FTIR Shimadzu IRAffinity-1S spectrometer equipped with an ATR ZnSe Performance Crystal Plate accessory with an average of 64 scans and 2 cm^{-1} of spectral resolution. The thermogravimetric data were recorded on a Shimadzu DTG60 thermobalance with a heating rate of 5 °C min^{-1} to a temperature of 500 °C in an air flow.

Powder X-Ray diffraction. The powder X-ray diffraction (PXRD) data for the compounds **1**−**3** were obtained on a D8 Advance diffractometer with Cu-*Kα* (λ= 1.54056 Å), operated at 40 kV and 30 mA, with a Ni filter and LynxEye linear detector. The diffractograms were collected in the 2θ angular range from 5° to 50°, with a step size of 0.02° and counting time ranging from 0.5 to 1 s per step with a divergence slit of 0.6 mm and primary/secondary Soller slits of 2.5°. Comparison of simulated and experimental diffractograms was used to confirm the purity of the microcrystalline products (Figures S6−S8).

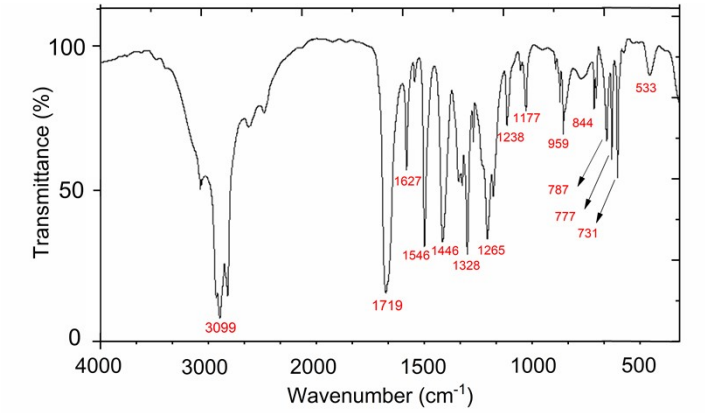

Figure S2. FTIR−ATR spectrum of 5-nitroisophthalic acid.[1]

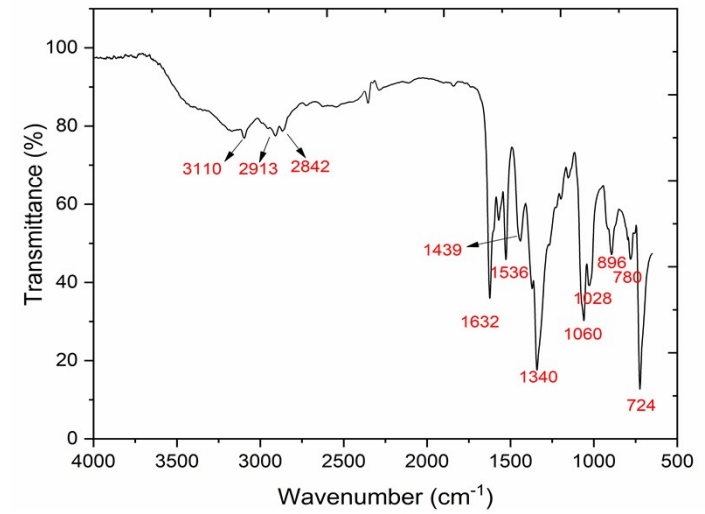

Figure S3. FTIR−ATR spectrum of **1**.

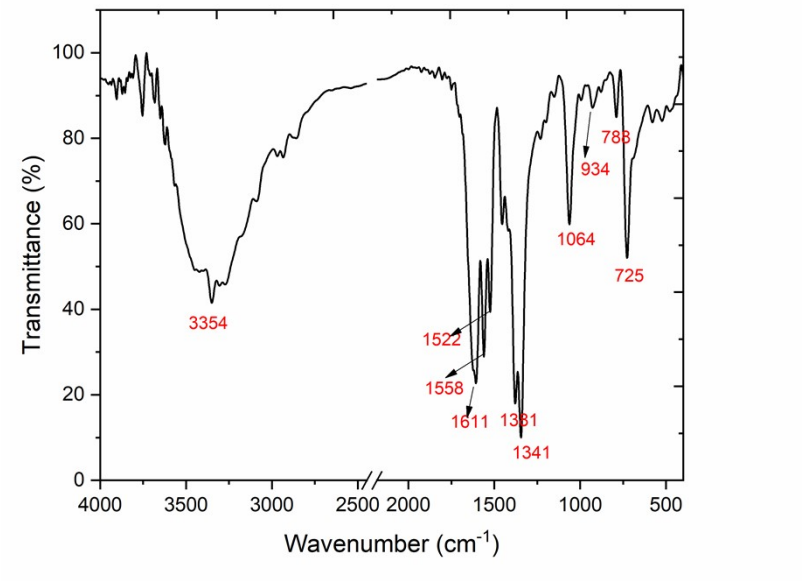

Figure S4. FTIR−ATR spectrum of **2**.

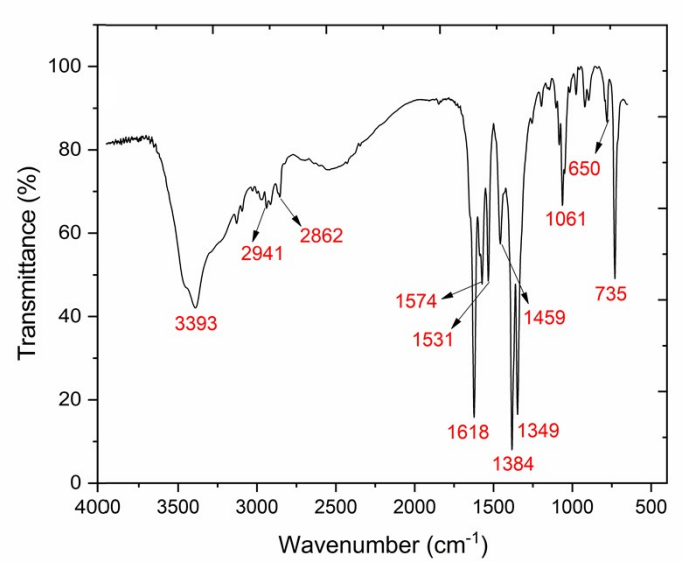

Figure S5. FTIR−ATR spectrum of **3**.

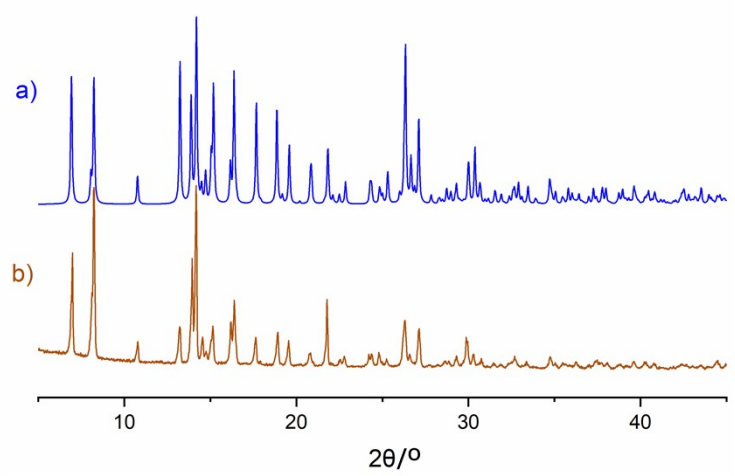

Figure S6. PXRD patterns of **1**: (a) simulated and (b) experimental.

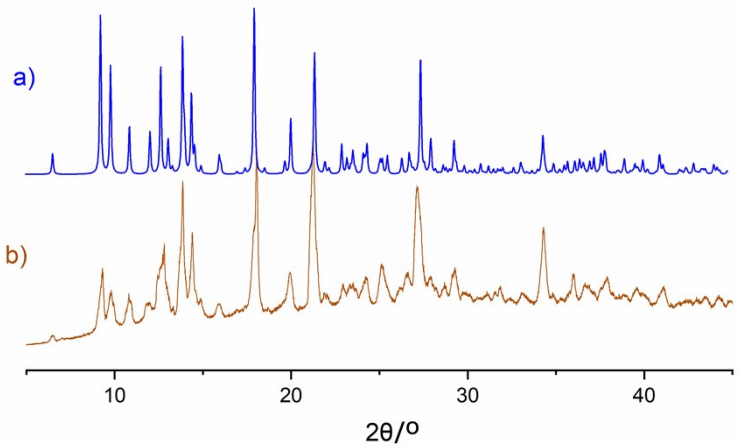

Figure S7. PXRD patterns of **2**: (a) simulated and (b) experimental.

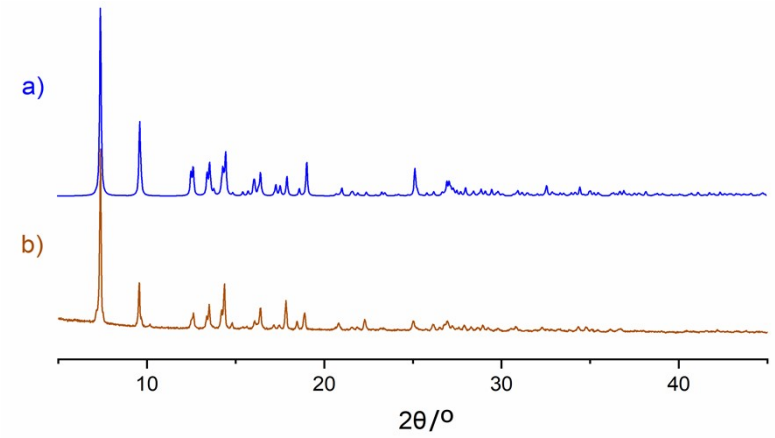

Figure S8. PXRD patterns of **3**: (a) simulated and (b) experimental.

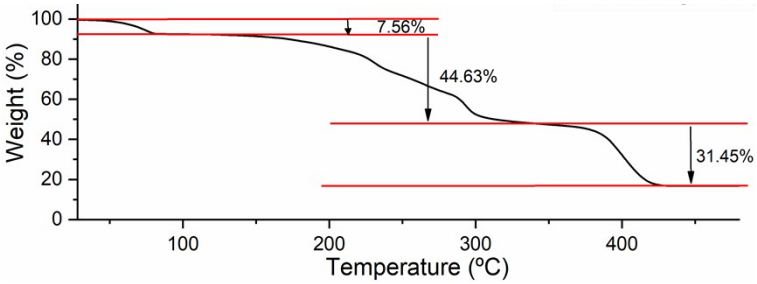

Figure S9. Thermogravimetric analysis of **1**.

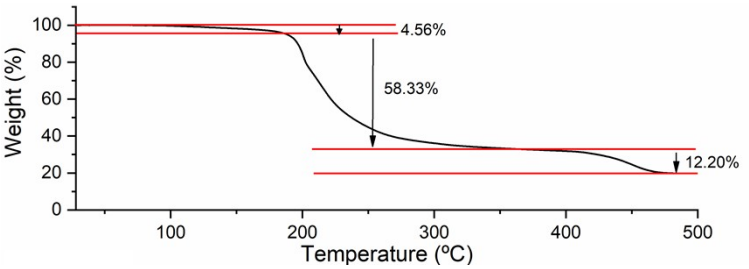

Figure S10. Thermogravimetric analysis of **2**.

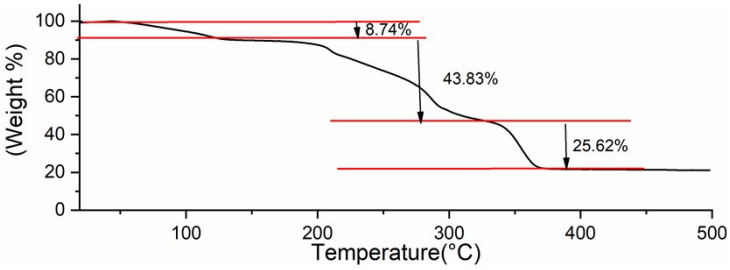

Figure S11. Thermogravimetric analysis of **3**.

Single crystal X-ray diffraction measurements. For compounds **1**, **2**, and **3**, suitable single crystals were selected for X-ray data collection on a Bruker APEX-II CCD diffractometer with a Mo-*Ka* radiation (λ = 0.71073 Å). Data reduction, scaling, and absorption corrections were performed using SAINT v8.37A.[2] The crystal structure of **1** was solved with the SHELXT 2014/5[3] program by Intrinsic Phase with Olex2 [4] as the graphical interface and refined with the SHELXL 2019/3 [5] using the full matrix least-squares minimisation on F^2. All non-hydrogen atoms were refined anisotropically. Hydrogen atom positions were calculated geometrically (C−H = 0.87–0.98 Å) and refined using the riding model with $U_{iso}(H) = 1.2U_{eq}(C)$ or $1.5U_{eq}(C)$ for H bonded to oxygen atoms. The proposed molecular formula considers the additional hydrogen atoms that were not possible to locate in the electron density map, as it disregards some disorder effects. CCDC codes 2386078-2386080.

Detailed structural description. The X−ray crystallographic details for **1**−**3** are given in Table S1, while the selected geometric parameters (bond and angles) can be found in Tables S2−S7. The crystal structure of $[Cu(H_3tea)(H_2O)_2(nipa)]\cdot H_2O$ (**1**) (Figure 2) is characterized by the presence of a $[Cu(H_3tea)(H_2O)_2]^{2+}$ cation and a $nipa^{2-}$ anion. In the cation, the Cu(II) center is 6-coordinated with a $\{CuO_5N\}$ environment, which is filled with one H_3tea ligand (Cu−O8 2.324(4) Å, Cu−O9 1.998(4) Å, Cu−O10 2.025(4) Å, and Cu−N1 2.009(4) Å) and two coordinated water molecules (Cu−O11 1.946(5) Å and Cu−O12 2.446(5) Å) in a non-centrosymmetric relation. The elongated bond lengths along the O8–Cu–O12 axis are typical for extensively stretched bonds, thus characterizing the Cu(II) coordination geometry as a strongly distorted octahedron, aligning with the Jahn-Teller distortion (Figure S12a). This distortion, observed in similar compounds in the literature,[6-8] can promote the redistribution of electrons between the metal center and the ligands, thus weakening some bonds with a possibility to favor the reactivity in the oxidative catalytic cycle.[9, 10] Additionally, the $nipa^{2-}$ anions accept weak hydrogen bonds from the adjacent $[Cu(H_3tea)(H_2O)_2]^{2+}$ cations, resulting in a structure stabilizing effect (Figure S12). When simplifying the H-bonded network in **1** to understand the contribution of strong hydrogen bonds [d(D···A) ≤ 2.50 Å; D—H···A ≥ 120°], the crystal structure is organized into a 2D network. It is run along the *bc* plane through H-bond motifs linked to each other by an O–H···O in the form $R_4^2(12)$ graph set[11] and stacks along the crystallographic *a* axis (Figure S12b). Based on viewing the H-bonded motifs from a topological perspective, there is the formation of a 2D net with an **sql** topology.[12,13]

Table S1. Crystal data and structure refinement for **1**, **2** and **3**.

Compound	**1**	**2**	**3**
Formula	$[Cu(H_3tea)(H_2O)_2](nipa)\cdot H_2O]$	$\{[Cu_2(\mu_3\text{-dap})(\mu\text{-Hnipa})(\mu_3\text{-nipa})(H_2O)]\cdot H_2O\}_n$	$\{[Cu_3(\mu_3\text{-Hmdea})_2(\mu_4\text{-nipa})(nipa)(H_2O)_3]\}_n$
Formula Weight	475.89	649.42	896.2
Crystal System	Monoclinic	Triclinic,	Triclinic
Space Group	$P2_1/c$	*P−1*	*P−1*
a / Å	12.720 (4)	8.169 (3)	7.3749 (10)

b / Å	21.515 (7)	9.891 (5)	13.1591 (14)
c / Å	7.046 (2)	14.098 (6)	19.230 (3)
α / °	90	105.24 (2)	104.287 (4)
β / °	92.062 (12)	96.014 (15)	96.867(5)
γ / °	90	90.575 (15)	103.278 (4)
V / Å^3	1927.0 (10)	1092.1(8)	1729.1 (4)
Z	4	2	2
Radiation type	MoK_a	MoK_a	MoK_a
μ (mm^{-1})	1.20	2.04	1.92
No. of measured, independent and observed [I > 2σ(I)] reflections	14143, 3523, 1933	22581, 3991, 2811	35596, 6313, 4469
R_{int}	0.128	0.098	0.080
Parameters	278	366	465
Restraints	9	22	19
R_1	0.067	0.066	0.065
wR_2	0.170	0.185	0.198
S	0.96	1.06	1.03
$\Delta\rho_{max}$, $\Delta\rho_{min}$ (e Å^{-3})	0.51, −1.05	0.78, −1.01	1.94, −1.27

The crystal structure analysis of {[Cu_2(μ$_3$-dap)(μ-Hnipa)(μ$_4$-nipa)(H_2O)]·H_2O}$_n$ (**2**) revealed the formation of a 1D coordination polymer composed of dicopper(II) [Cu_2(μ$_3$-dap)(μ-Hnipa)(H_2O)]$^{2+}$ secondary building units (SBUs) and μ$_4$-nipa^{2-} linkers (Figure S13). The Cu1 center adopts an almost ideal square-pyramidal {$CuNO_4$} environment as suggested by the index geometry parameters.[14-16] Particularly, Cu1 has a geometry index (*τ5*) equal to 0.03 (*β* and *α* are the valence angles of 170.2(3) and 168.3(3)°, respectively). Despite showing a 6-coordinate {$CuNO_5$} environment, the Cu2 center has a resembling geometry due to the elongation of the Cu2−O8 bond [2.69(8) Å] with a *τ5* parameter of 0.04 (*β* = 174.4(3) and *α* = 172.0(3)°; Figure 2b). For compound **2**, the typical average Cu−O and Cu−N bond lengths are 2.16(5) and 1.99(7) Å, respectively, being in agreement with expected range for nipa-based compounds.[17] As a result, the SBUs are extended by μ$_4$-nipa^{2-} linkers along the crystallographic *a* axis, forming a 1D coordination polymer with a 3x5 Å window-opening channel (Figure S13b).

The compound {[Cu_3(μ$_3$-Hmdea)$_2$(μ$_4$-nipa)(nipa)(H_2O)$_3$]}$_n$ (**3**) is also a 1D coordination polymer (Figure S14). Its structure is distinguished by the presence of two different trinuclear copper(II) SBUs (*i* and *ii*), that are interlinked via μ$_4$-nipa^{2-} bridging ligands (Figure S14a). Within the trinuclear units,

the copper(II) atoms exhibit distinct geometries, with the central atoms (Cu3/Cu5) displaying an elongation of Cu−O (Cu3−O7 2.670(5) Å and Cu5−O19 2.529(6) Å) bonds induced by the Jahn-Teller effect in relation to water molecules and free $nipa^{2-}$ ligands in the network, creating a type of (4+2) coordination (Figure S14a).[8] As mentioned earlier, there are two alternating types of trinuclear units in the structure that can be found, namely $[Cu_3(\mu_3\text{-Hmdea})_2(H_2O)_4]^{4+}$ (*i*) and $[Cu_3(\mu_3\text{-Hmdea})_2(nipa)_2]$ (*ii*). In the $[Cu_3(\mu_3\text{-Hmdea})_2(H_2O)_4]^{4+}$ SBU (*i*), the Cu4 center adopts a distorted square-pyramidal {CuO_4N} geometry [$\tau 5 = 0.16$, β and α valence angles of 174.0(2)° and 164.2(2)°, respectively]. In the neutral $[Cu_3(\mu\text{-Hmdea})_2(nipa)_2]$ unit, the copper atoms Cu1 and Cu2 atoms exhibit positional disorder in a 60:40 ratio (inset, Figure S14a). Nonetheless, the central atom, Cu2 atom adopts a similar distorted square-pyramidal geometry [$\tau 5 = 0.31$; $\beta = 169.4(3)°$ and $\alpha = 150.6(3)°$]. The average bond distances, d_{avg}(Cu−O) = 1.99(5) Å and d_{avg}(Cu−N) = 1.97(6) Å, are within the normal values for this type of compounds.[17] A simplified 1D network in **3** reveals a 2C1 topology, with the trinuclear units acting as network nodes (Figure S14c).

Table S2. Selected Bond Lengths (**Å**) in **1**.

Bond	***Length***	***Bond***	***Length***
Cu1—O9	1.998 (4)	O2—C8	1.283 (7)
Cu1—O8	2.324 (4)	O1—C8	1.237 (7)
Cu1—O10	2.025 (4)	O4—C7	1.259 (7)
Cu1—N1	2.009 (5)	O3—C7	1.256 (7)
Cu1—O11	1.946 (5)	O6—N2	1.224 (7)
Cu1—O12	2.446 (5)	O5—N2	1.239 (7)

Table S3. Selected Bond Angles (°) in **1**.

Atoms	***Angle***	***Atoms***	***Angle***
O9—Cu1—O8	91.55 (17)	O11—Cu1—O8	94.14 (19)
O9—Cu1—O10	165.62 (18)	O11—Cu1—O10	96.5 (2)
O9—Cu1—N1	84.69 (19)	O11—Cu1—N1	176.5 (2)
O10—Cu1—O8	95.39 (16)	O6—N2—O5	123.5 (6)
N1—Cu1—O8	82.35 (18)	O1—C8—O2	123.9 (6)
N1—Cu1—O10	83.8 (2)	O3—C7—O4	123.8 (6)
O11—Cu1—O9	95.51 (19)		

Table S4. Selected Bond Lengths (**Å**) in **2**.

Bonds	***Length***	***Bonds***	***Length***
Cu2—O4^{i}	1.961 (5)	O2—C1	1.229 (9)
Cu2—O13	1.921 (5)	O3—C8	1.246 (8)
Cu2—O14	1.993 (6)	O4—C8	1.262 (8)
Cu2—N4	1.990 (7)	O6—N1	1.212 (9)
Cu1—N3	1.987 (7)	O5—N1	1.217 (9)
Cu1—O1	1.932 (5)	O9—C17	1.271 (18)
Cu1—O3i	1.964 (5)	O8—C9	1.325 (17)
Cu1—O13	1.915 (5)	O7—C9	1.372 (17)
O1—C1	1.264 (9)	C17—O10	1.22 (2)
Symmetry code: (i) $-x+1, -y+1, -z+1$.			

Table S5. Selected Bond Angles (°) in **2**.

Atoms	*Angle*	*Atoms*	*Angle*
O4^{i}—Cu2—O14	90.4 (3)	O3^{i}—Cu1—N3	170.2 (3)
O4i—Cu2—N4	174.4 (3)	O13—Cu1—N3	84.0 (2)
O13—Cu2—O4i	94.2 (2)	O13—Cu1—O1	168.3 (3)
O13—Cu2—O14	172.0 (3)	O13—Cu1—O3i	92.0 (2)
O13—Cu2—N4	85.0 (3)	O2—C1—O1	126.3 (7)
N4—Cu2—O14	91.1 (3)	O3—C8—O4	128.1 (7)
O1—Cu1—N3	95.8 (2)	O6—N1—O5	124.1 (7)
O1—Cu1—O3i	86.4 (2)	O8—C9—O7	129.1 (12)
Symmetry code: (i) −*x*+1, −*y*+1, −*z*+1.			

Table S6. Selected Bond Lengths (**Å**) in **3**.

Bonds	*Length*	*Bonds*	*Length*
Cu3—O1	1.990 (4)	Cu4—O18	2.422 (10)
Cu3—O14	1.927 (5)	O1—C1	1.248 (7)
Cu3—O7	2.670 (5)	O2—C1	1.243 (8)
Cu2—O2	1.829 (5)	O2—Cu1	2.259 (5)
Cu2—O14	1.941 (5)	O3—C8	1.242 (8)
Cu2—O17	2.343 (7)	O4—C8	1.260 (8)
Cu2—N1	1.933 (6)	O5—N3	1.210 (9)
Cu2—O13	1.997 (9)	O9—C16	1.267 (8)
Cu2—O15	2.102 (13)	O11—N4	1.227 (9)
Cu5—O3	1.995 (4)	O10—C16	1.249 (8)
Cu5—O20	1.939 (5)	O17—Cu1	1.797 (7)
Cu5—O19	2.529 (6)	N1—Cu1	1.975 (7)
Cu4—O20	1.917 (5)	N3—O6	1.205 (9)
Cu4—O4	1.918 (4)	O12—N4	1.207 (10)
Cu4—N2	2.009 (6)	O13—Cu1	2.218 (9)
Cu4—O16	1.973 (5)	Cu1—O15	1.991 (12)

Table S7. Selected Bond Angles (°) in **3**.

Atoms	*Angle/°*	*Atoms*	*Angle/°*
O1^{i}—Cu3—O1	180.0	O20—Cu5—O3	89.00 (19)
O14^{i}—Cu3—O1	88.05 (19)	O20^{ii}—Cu5—O20	180.0 (3)
O14—Cu3—O1	91.95 (19)	O20—Cu4—O4	97.0 (2)
O14—Cu3—O14^{i}	180.0	O20—Cu4—N2	88.7 (2)
O2—Cu2—O14	102.1 (2)	O20—Cu4—O16	164.2 (2)
O2—Cu2—O17	97.9 (3)	O20—Cu4—O18	101.5 (3)
O2—Cu2—N1	150.6 (3)	O4—Cu4—N2	174.0 (2)
O2—Cu2—O13	87.0 (3)	O4—Cu4—O16	91.8 (2)
O2—Cu2—O15	102.9 (4)	O4—Cu4—O18	88.4 (3)
O14—Cu2—O17	87.9 (3)	N2—Cu4—O18	88.7 (4)
O14—Cu2—O13	169.4 (3)	O16—Cu4—N2	83.1 (2)
O14—Cu2—O15	147.8 (5)	O16—Cu4—O18	91.8 (3)
N1—Cu2—O14	87.3 (2)	O14—Cu1—O2	88.9 (2)
N1—Cu2—O17	110.4 (3)	O14—Cu1—N1	86.9 (3)
N1—Cu2—O13	82.1 (3)	O14—Cu1—O13	143.2 (4)
N1—Cu2—O15	80.8 (4)	O14—Cu1—O15	168.9 (5)
O13—Cu2—O17	96.4 (4)	O17—Cu1—O2	101.9 (3)
O13—Cu2—O15	30.5 (4)	O17—Cu1—O14	107.3 (3)
Cu1—Cu2—O2	124.8 (5)	O17—Cu1—N1	137.7 (4)
Cu1—Cu2—O14	77.9 (4)	O17—Cu1—O13	107.3 (4)

Cu1—Cu2—O17	27.5 (4)	O17—Cu1—O15	83.2 (5)
Cu1—Cu2—N1	84.2 (5)	N1—Cu1—O2	118.4 (3)
Cu1—Cu2—O13	101.6 (6)	N1—Cu1—O13	75.8 (3)
Cu1—Cu2—O15	71.2 (6)	N1—Cu1—O15	82.7 (4)
O15—Cu2—O17	68.8 (5)	O13—Cu1—O2	72.1 (3)
$O3^{ii}$—Cu5—O3	180.0	O15—Cu1—O2	92.7 (5)
$O20^{ii}$—Cu5—O3	91.00 (18)	O15—Cu1—O13	29.1 (5)

Symmetry codes: (i) −x, −y+1, −z; (ii) −x+2, −y+2, −z+1.

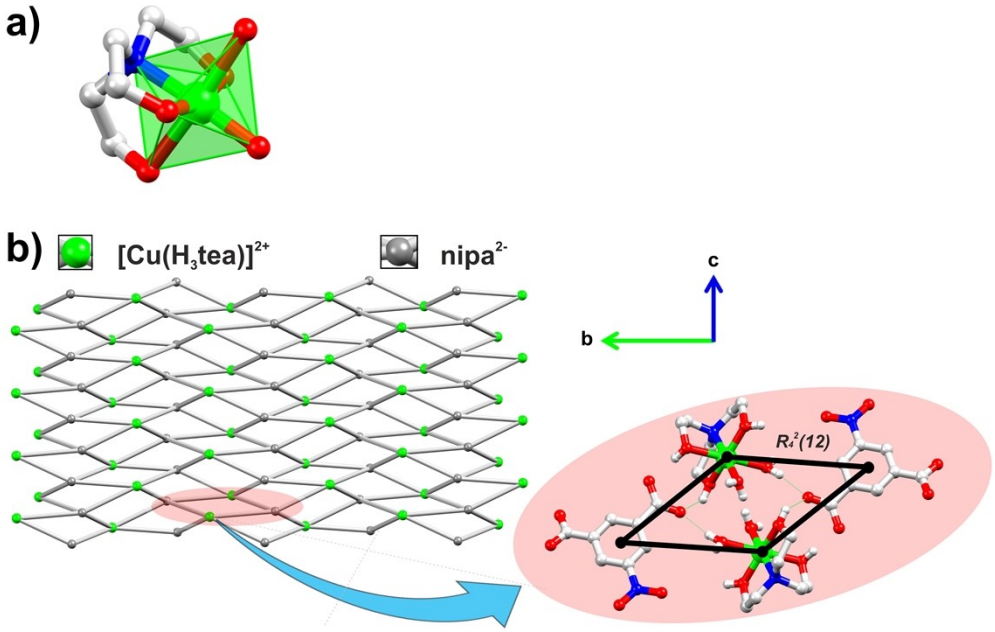

Figure S12. (a) Polyhedral representation of mononuclear copper(II) units, $[Cu(H_3tea)]^{2+}$, with octahedral geometry. (b) Representation of the 2D network involving H-bond motifs linked to each other along the *bc* plane in compound **1**. Color codes: Cu green balls, O red, N blue, C gray.

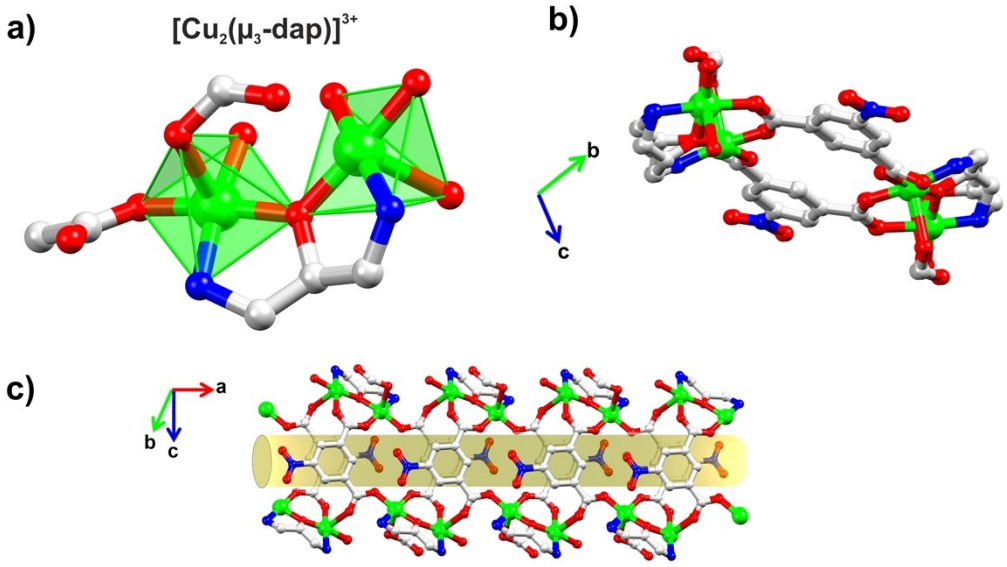

Figure S13. (a) Polyhedral representation of dinuclear copper(II) units, $[Cu2(dap)]^{3+}$, with square pyramidal geometry. (c) Representation of a 3×5 Å window-opening channel, forming a tubular 1D framework along the *bc* crystallographic axis. (c) Tubular framework along the a axis. Disordered atoms, ligands, solvent molecules, and hydrogen atoms are omitted for clarity. Color codes: Cu: green; O: red; N: blue; C: gray.

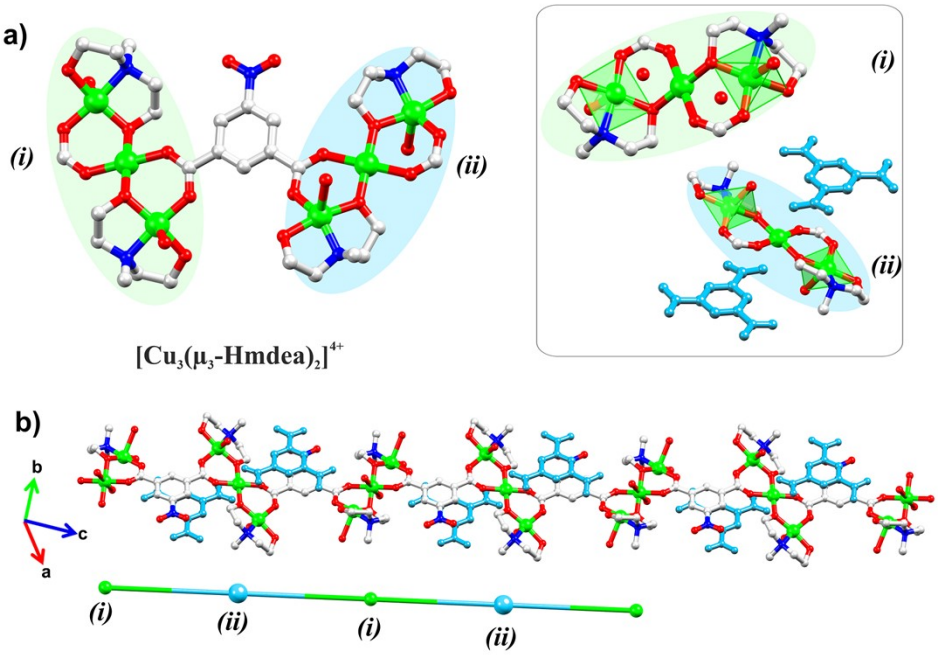

Figure S14. (a) Representation of tricopper(II) units in compound **3**. Inset: Different trinuclear copper(II) units $[Cu_3(\mu_3\text{-Hmdea})_2]^{4+}$, (*i*): $[Cu_3(\mu_3\text{-Hmdea})(H_2O)_2]^{4+}$ and (*ii*): $[Cu_3(\mu_3\text{-Hmdea})(nipa)_2]$, through polyhedral representation. (b) Extension into a 1D coordination polymer chain via μ_4-$nipa^{2-}$ linkers. Disordered ligands, solvent molecules and H atoms are omitted for clarity. Color codes: Cu: green; O: red; N: blue; C: gray.

Section 2 – Catalytic Studies

Oxidation of α-pinene: The GC (gas chromatography) analyses were performed on an Agilent Technologies 7820A series gas chromatograph (carrier gas, helium; detector, flame ionization; capillary column, BP20/SGE, 30 m × 0.22 mm × 0.25 μm). The crude reaction mixture was diluted in 1 mL acetonitrile, followed by the addition of nitromethane (71 μL, 1.32 mmol) as an internal standard. This final mixture was diluted in 1:4 acetonitrile and 1 μL was injected at a temperature of 280 °C and 1:50 split ratio. The temperature program was 100 °C for 6 min and then 10 °C min^{-1} until 180°C. For characterization of unidentified compounds, GC−MS analyses were performed on a Scion 436−GC equipped with a polar BP20/SGE column (30 m × 0.25 mm × 0.25 μm), an electron impact ionization source, and a simple quadrupole analyser.

The number of mols (*n*) of α-pinene, pinene oxide, and verbenone was determined by using calibration curves, in which the angular coefficients (*a*) were 10.93, 9.38, and 9.50, respectively. However, for *tert*-butylperoxy-2-pinene, which is not commercially available, the inverse function of angular coefficient was determined by correlation between the peak area of the isolated product (0.12 mmol) and verbenone (0.12mmol), i.e., $\left(\frac{1}{a}\right)_{tert-butylperoxy-2-pinene} = 1.62 \times \left(\frac{1}{a}\right)_{Verbenone}$.

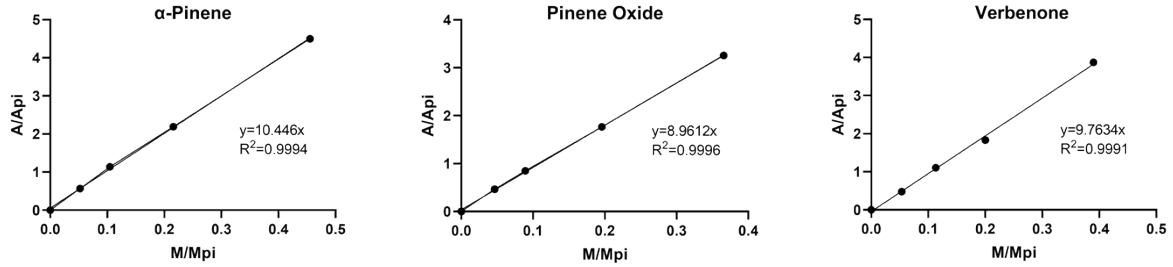

Figure S15. Calibration curves for α-pinene, pinene oxide and verbenone.

$$n = \frac{A}{A_{IS}} \cdot \left(\frac{1}{a}\right) \cdot n_{IS}$$

Equation 1

A − peak area
n – number of mols
a – angular coefficient
A_{IS} − peak area of internal standard
n_{IS} – number of mols of internal standard

Characterization of GC reference products by Nuclear Magnetic Resonance (NMR). The solution ^1H spectra were obtained on a 500 MHz and 400 MHz NMR spectrometers (Varian Inc.), using deuterated chloroform as solvent. The chemical shifts (δ) are relative to tetramethylsilane (TMS), used as the internal standard.

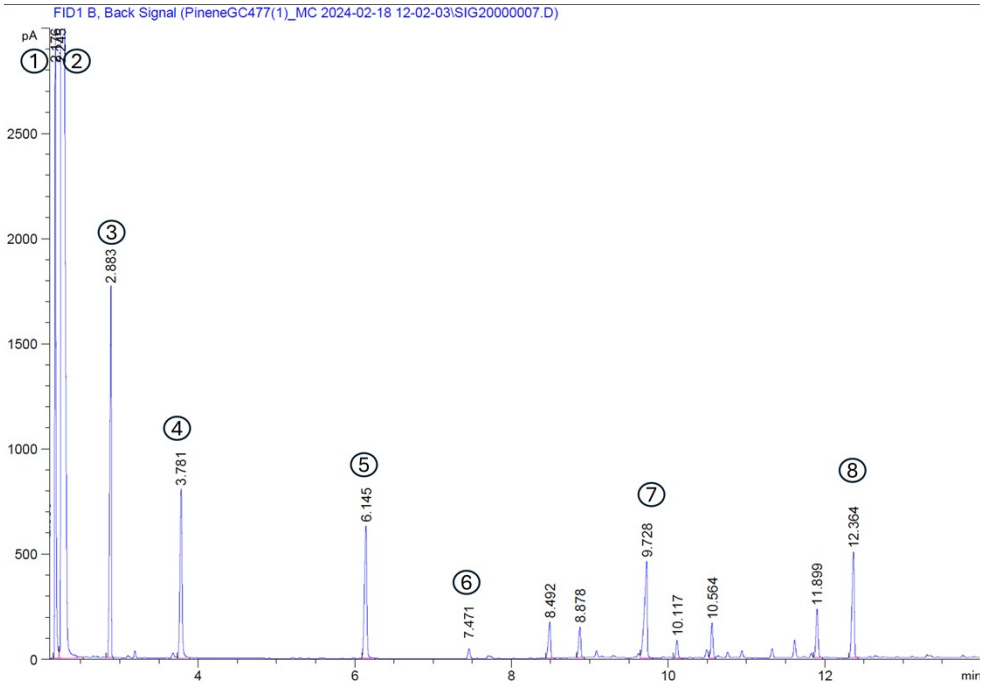

Figure S16. Typical gas chromatogram of the reaction mixture in Cu-catalyzed oxidation of α-pinene. Conditions: α-pinene (0.6 mmol), catalyst (6 μmol), TBHP (70% in H_2O, 1.2 mmol), PS-750-M (1% water solution, 1 mL), 1500 rpm, 60 °C. Identification: (1) *tert*–BuOH, (2) EtOAc, (3) α-pinene, (4) nitromethane (GC standard), (5) TBHP, (6) pinene oxide, (7) *tert*-butylperoxy-2-pinene, (8) verbenone.

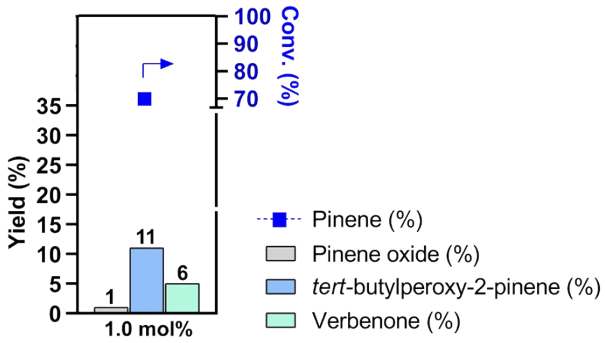

Figure S17. Oxidation of α-pinene with TBHP under micellar conditions in the presence of **3**. Conditions: α-pinene (0.6 mmol), catalyst (0.5–2.0 mol%), TBHP (70% in H_2O, 1.2 mmol), PS-750-M (1% in H_2O, 1 mL), 6 h, 1500 rpm, 60 °C.

Table S8. Cu-catalyzed oxidation of α-pinene catalyzed by **1**, **2** and **3** (effect of catalyst loading).[a]

Entry	Catalyst	Amount (mol%)[b]	Conversion (%)[c]	Yield of the main products (%)[d]			
			A	**B**	**C**	**D**	**Total**
1	**1**	0.5	69.0	11.0	5.5	2.0	**17.5**
2		1.0	78.5	24.5	13.5	7.0	**45.0**
3		2.0	87.0	25.5	16.0	5.0	**46.5**
4	**2**	0.5	75.0	11.0	6.0	3.0	**20.0**
5		1.0	77.5	18.5	10.0	3.0	**31.5**
6		2.0	85.5	22.0	14.5	4.0	**40.5**
7	**3**	1.0	68.0	9.0	4.5	3.0	**16.5**

[a]Conditions: α-pinene (0.6 mmol), catalyst (**1**−**3,** ranging 0.5−2.0 mol%), TBHP (70% in H_2O; 1.2 mmol), PS-750-M (1% in H_2O, 1 mL), 6 h, 1500 rpm, 60 °C. [b] *mol%*: [moles of catalyst / (moles of catalyst + moles of α-pinene) × 100]. [c]*Conversion*: [moles of α-pinene initial − moles of α-pinene final) / (moles of α-pinene) × 100]. [d]*Yield* was determined by GC based on α-pinene: (moles of product per initial mol of α-pinene) × 100. (A: α-pinene; B: *tert*-butylperoxy-2-pinene; C: verbenone; D: pinene oxide). 0.00

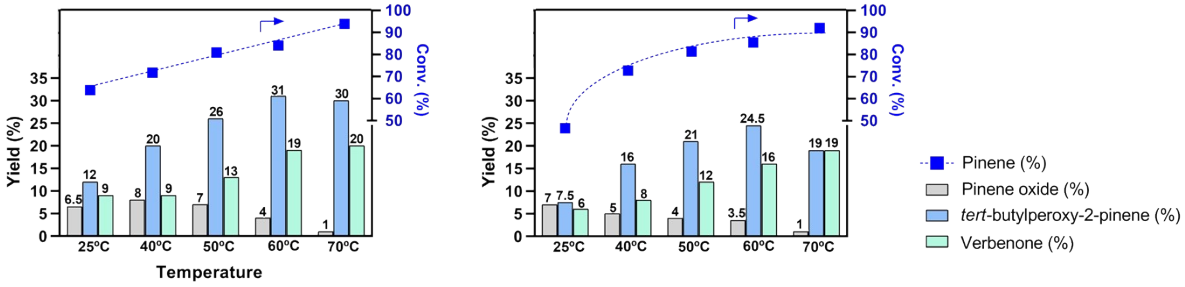

Figure S18. Cu-catalyzed oxidation of α-pinene over **1** (left) and **2** (right), at temperature ranging from 25 to 70 ºC. Conditions: α-pinene (0.6 mmol), catalyst (1.0 mol%), TBHP (70% in H_2O, 1.2 mmol), PS-750-M (1% in H_2O; 1 mL), 9 h, 1500 rpm, 60 °C.

Table S9. Cu-catalyzed oxidation of α-pinene catalyzed by **1** and **2** (effect of temperature).[a]

Entry	Temperature (°C)	Catalyst	Conversion (%)[b]	Yield of the main products (%)[c]			
			A	**B**	**C**	**D**	**Total**
1	25		64.0	12.0	9.0	6.5	27.5
2	40		71.0	20.0	9.0	8.0	37.0
3	50	**1**	80.0	26.0	13.0	7.0	46.0
4	60		87.5	31.0	19.0	4.0	54.0
5	70		94.0	30.0	20.0	1.0	51.0
6	25		43.5	7.5	6.0	7.0	20.5
7	40		57.0	16.0	8.0	5.0	29.0
8	50	**2**	77.0	21.0	12.0	4.0	37.0
9	60		87.0	24.5	16.0	3.5	44.0
10	70		91.0	19.0	19.0	1.0	39.0

[a]Conditions: α-pinene (0.6 mmol), catalysts (**1** and **2**; 1.0 mol%), TBHP (70% in H_2O; 1.2 mmol), PS-750-M 1 % H_2O (1 mL), 9h, 1500 rpm, temperature (25−60°C). [b] *Conversion*: [moles of α-pinene initial − moles of α-pinene final) / (moles of α-pinene) × 100]. [c] *Yield* was determined by GC based on α-pinene: (moles of product per initial mol of α-pinene) × 100. (A: α-pinene; B: *tert*-butylperoxy-2-pinene; C: verbenone; D: pinene oxide).

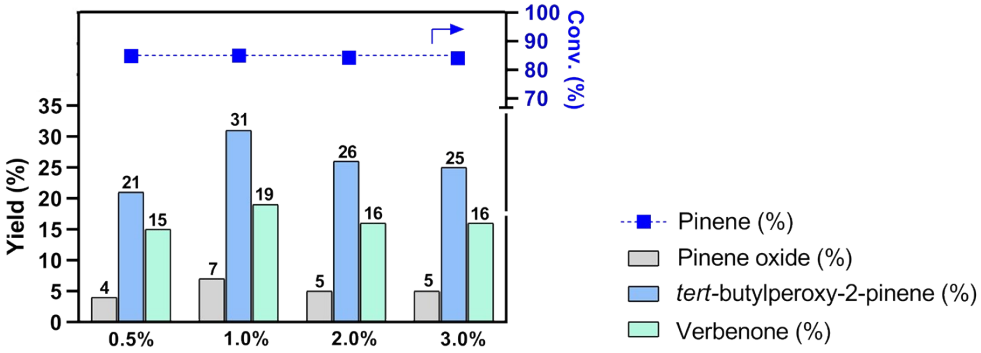

Figure S19. Cu-catalyzed oxidation of α-pinene over **1**. Effect of the concentration of PS-750-M in water (0.5−3.0%). Conditions: α-pinene (0.6 mmol), catalyst (1.0 mol%), TBHP (70% in H_2O, 1.2 mmol), PS-750-M (0.5−3.0% in H_2O, 1 mL), 9 h, 1500 rpm, 60 °C.

Table S10. Cu-catalyzed oxidation of α-pinene catalyzed by **1** (effect of surfactant concentration). [a]

Entry	Amount of PS-750-M (%)[b]	Conversion (%)[c]	Yield of the main products (%)[d]			
		A	**B**	**C**	**D**	**Total**
1	0.5	88.5	21.0	15.0	4.0	40.0
2	1.0	87.0	31.0	19.0	4.0	54.0
3	2.0	85.0	27.5	16.5	5.0	49.0
4	3.0	84.5	26.5	16.0	5.0	47.5

[a]Conditions: α-pinene (0.6 mmol), Catalyst **1** (1.0 mol%), TBHP (70% in H_2O; 1.2 mmol), PS-750-M (0.5−3.0 % H_2O), 9h, 1500 rpm, 60 °C. [b] *mass%*: (mass of surfactant / (mass of surfactant + mass of H_2O) × 100]. [c]*Conversion:* [moles of α-pinene initial − moles of α-pinene final) / (moles of α-pinene) × 100]. [c] *Yield* was determined by GC based on α-pinene: (moles of product per initial mol of α-pinene) × 100. (A: α-pinene; B: *tert*-butylperoxy-2-pinene; C: verbenone; D: pinene oxide).

Table S11. Cu-catalyzed oxidation of α-pinene catalyzed by **1** (effect of oxidant-to-substrate molar ratio).[a]

Entry	TBHP:Pinene (Ratio)	Catalyst	Conversion (%)[b]	Yield of the main products (%)[c]			
			A	**B**	**C**	**D**	**Total**
1	2:1	**1**	87.0	31.0	19.0	4.0	54.0
2	3:1		86.0	27.0	18.0	6.0	51.0
3	2:1	**2**	87.5	24.5	16.5	3.0	44.0
4	3:1		88.5	25.5	14.5	3.5	43.5

[a]Conditions: α-pinene (0.6 mmol), catalyst (1.0 mol% of **1** and **2**), TBHP 70% H_2O (1.2−1.8 mmol), PS-750-M 1 % H_2O (1 mL), 9h, 1500 rpm, 60 °C. [b]*Conversion:* [moles of α-pinene initial − moles of α-pinene final) / (moles of α-pinene) × 100]. [c] *Yield* was determined by GC based on α-pinene: (moles of product per initial mol of α-pinene) × 100. (A: α-pinene; B: *tert*-butylperoxy-2-pinene; C: verbenone; D: pinene oxide).

Table S12. Cu-catalyzed oxidation of α-pinene catalyzed by **1** (effect of time).[a]

Entry	Time (h)	Conversion (%)[b]	Yield of the main products (%)[c]			
		A	**B**	**C**	**D**	**Total**
1	0.25	9.0	3.0	2.0	2.0	7.0
2	0.5	21.0	7.5	3.0	3.0	13.5
3	1.0	38.0	12.5	7.0	4.0	23.5
4	2.0	62.0	15.0	8.0	8.0	31.0
5	3.0	71.0	17.0	9.0	9.0	35.0
6	6.0	80.0	24.0	12.0	8.0	44.0
7	9.0	87.0	31.0	19.0	4.0	54.0
8	12.0	89.0	27.0	15.5	1.0	43.5
9	24.0	91.0	24.5	15.0	0.5	40.0

[a]Conditions: α-pinene (0.6 mmol), catalyst **1**, TBHP (70% in H_2O; 1.2 mmol), PS-750-M 1 % H_2O (1 mL), 24h, 1500 rpm, 60 °C. [b]*Conversion:* [moles of α-pinene initial − moles of α-pinene final) / (moles of α-pinene) × 100]. [c] *Yield* was determined by GC based on α-pinene: (moles of product per initial mol of α-pinene) × 100. (A: α-pinene; B: *tert*-butylperoxy-2-pinene; C: verbenone; D: pinene oxide).

Table S13. Comparative study in the oxidation of α-Pinene using distinct oxidative systems.[a]

Entry	Catalyst	Reaction Medium	Conversion (%)[b]	Yield of the main products (%)[c]			
			A	**B**	**C**	**D**	Total
1	−	H_2O	30.5	1.5	3.5	1.0	6.0
2[d]	**1**	H_2O	50.0	13.5	7.0	0.5	21.0
3	−	PS-750-M 1% H_2O[e]	43.0	8.0	5.5	1.0	14.5
4[d]	$Cu(NO_3)_2$	PS-750-M 1 % H_2O[e]	31.5	4.5	6.0	0.5	11.0
5[d]	**1**	PS-750-M 1 % H_2O[e]	87.0	31.0	19.0	4.0	54.0

[a] Conditions: α-pinene (0.6 mmol), catalyst (optional), TBHP (70% in H_2O; 1.2 mmol), PS-750-M 1 % H_2O (optional) 1 mL), 9h, 1500 rpm, 60 °C. [b] *Conversion:* [moles of α-pinene initial − moles of α-pinene final) / (moles of α-pinene) × 100]. [c] *Yield* was determined by GC based on α-pinene: (moles of product per initial mol of α-pinene) × 100. [d] Concentration of catalyst: 1.0 mol%. [e] *mass%*: (mass of surfactant / (mass of surfactant + mass of H_2O) × 100]. (A: α-pinene; B: tert-butylperoxy-2-pinene; C: verbenone; D: pinene oxide).

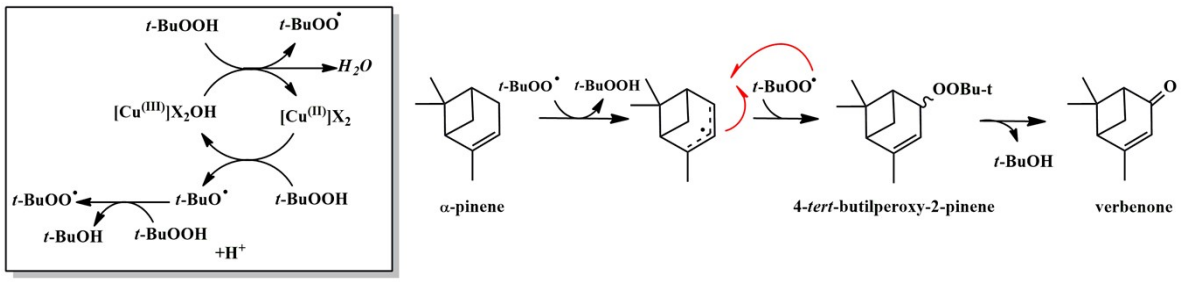

Scheme S1. Mechanistic proposal for the allylic oxidation α-pinene over Cu-based catalyst using TBHP as the oxidant.[18,19,20]

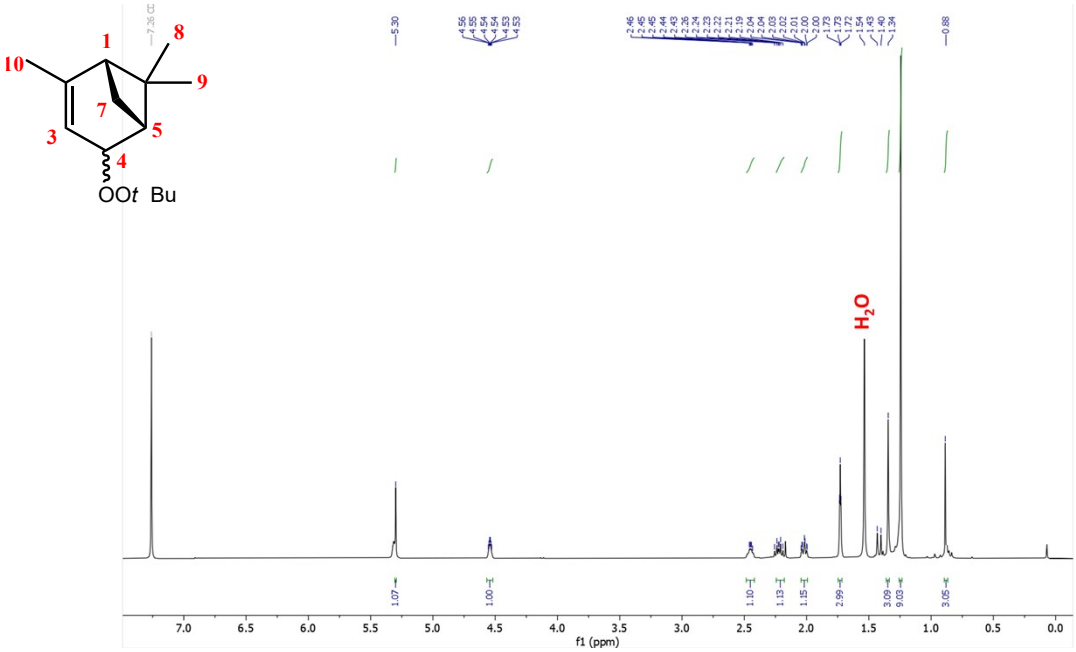

Figure S20. [1]H NMR spectrum of the isolated *tert*-butylperoxy-2-pinene in chloroform-d.

tert-butylperoxy-2-pinene: [1]H NMR ($CDCl_3$, 300 MHz) δ 0.88 (s, 3H, CH_3, H-9), 1.23 (s, 9H, *t*-Bu), 1.33 (s, 3H, CH_3, H-8), 1.40 (dt, 1H, H-7*exo*, J = 8.9, 1.4 Hz), 1.73 (t, 3H, CH_3, H-10, J = 1.7 Hz), 2.0 (td, 1H, H-1, J = 6.6, 1.6 Hz), 2.21 (dt, 1H, H-7, J = 8.9, 5.6 Hz), 2.45-2.50 (m, 1H, H-5), 4.52-4.56 (m, 1H, H-4), 5.30 (m, 1H, H-3).[21]

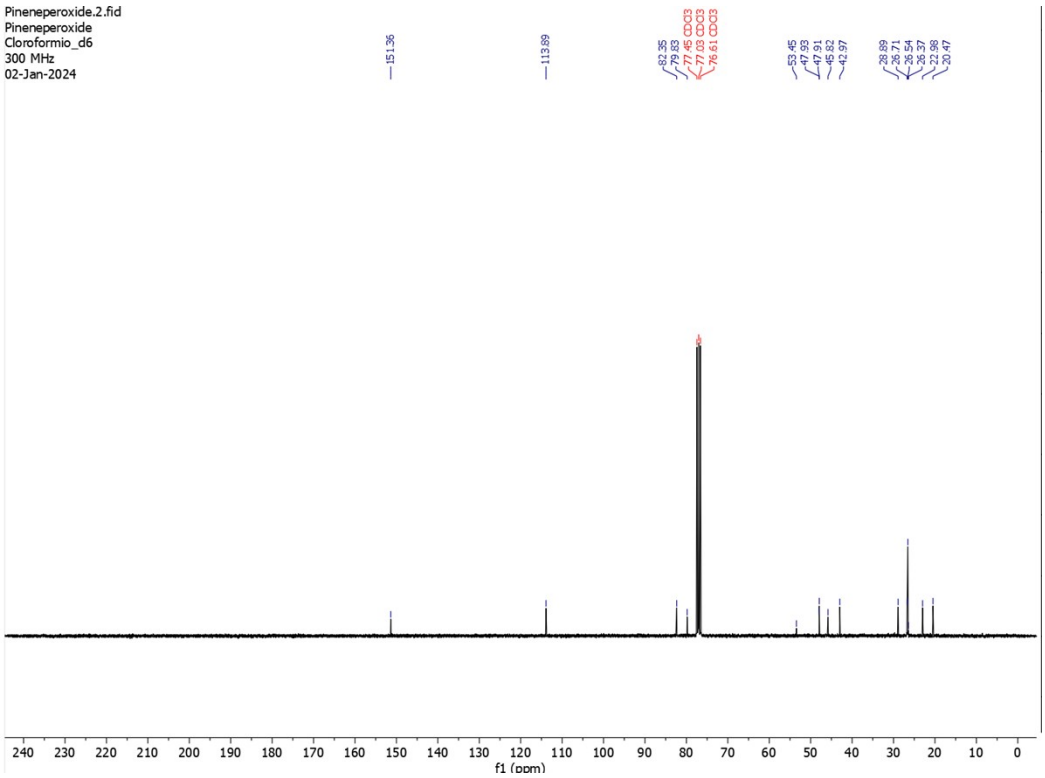

Figure S21. ^{13}C NMR spectrum of the isolated *tert*-butylperoxy-2-pinene in chloroform-d.

^{13}C NMR ($CDCl_3$, 75 MHz) δ 20.5 (C-9), 23.0 (C-10), 26.4 (*t*-Bu), 26.7 (C-8), 28.9 (C-7), 43.0 (C-5), 45.8 (C-6), 47.9 (C-1), 79.8 (C-O), 82.4 (C-4), 113.9 (C-3), 151.4 (C-2).[21]

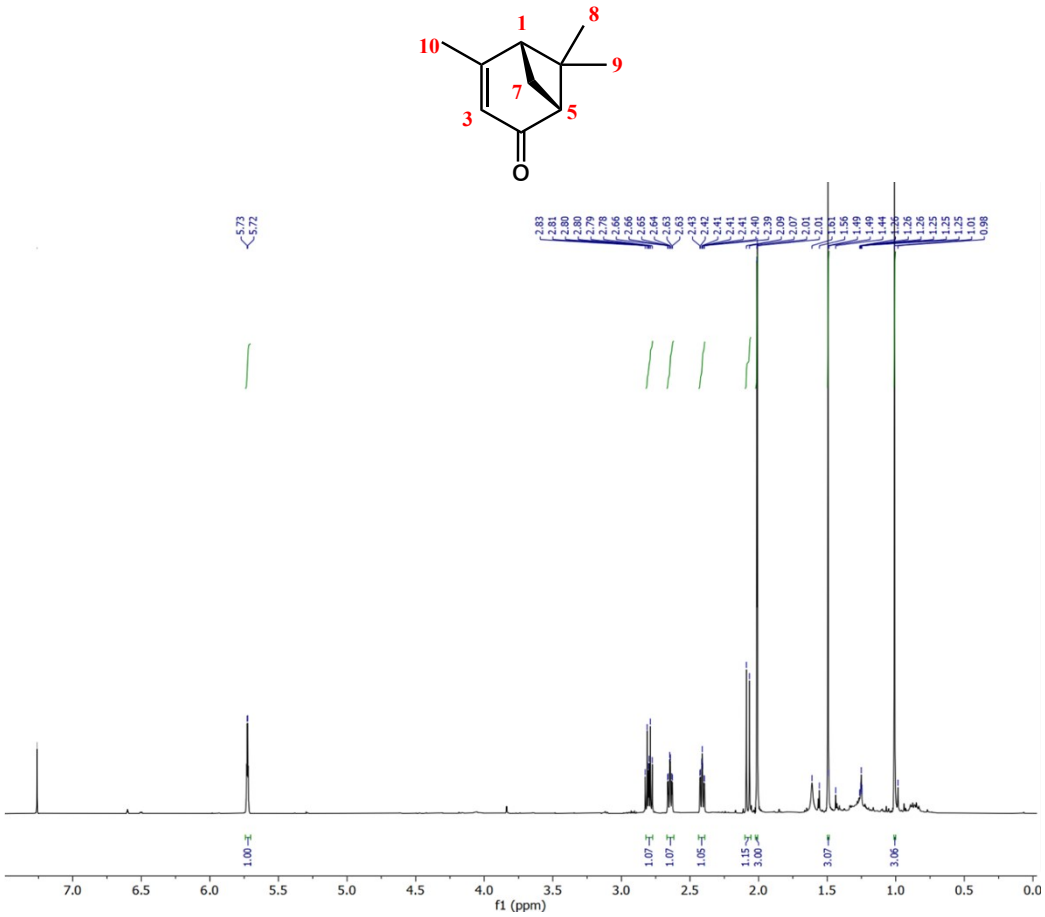

Figure S22. 1H NMR spectrum of verbenone.

Verbenone; 1H NMR ($CDCl_3$, 300 MHz) δ 1.00 (s, 3H, CH3, H-9), 1.49 (s, 3H, CH3, H-8), 2.01 (d, 3H, H-10, CH3, J = 1.5 Hz), 2.07 (d, 1H, H-1, J = 9.5 Hz), 2.39–2.41 (m, 1H, H-7), 2.63–2.66 (m, 1H, m), 2.77–2.83 (m, 1H, H-5), 5.72–5.73 (m, 1H, H-3).[22]

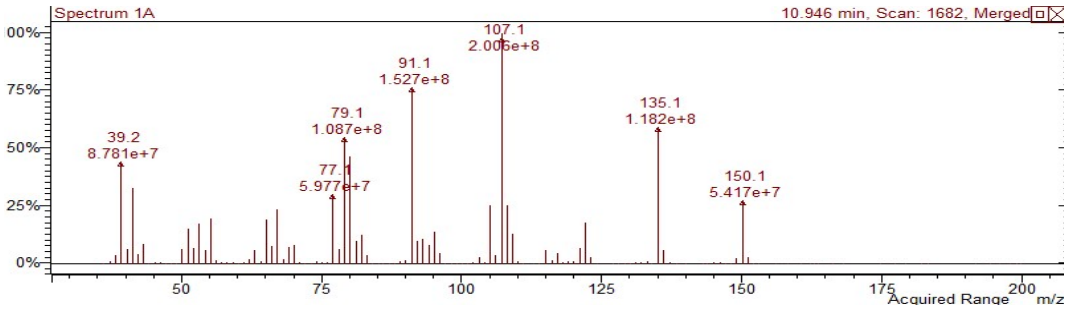

Figure S23. Mass spectrum of verbenone obtained in the oxidation of α-pinene. GC–MS (EI): *m/z* 150, 107 (C_4H_9O).[22]

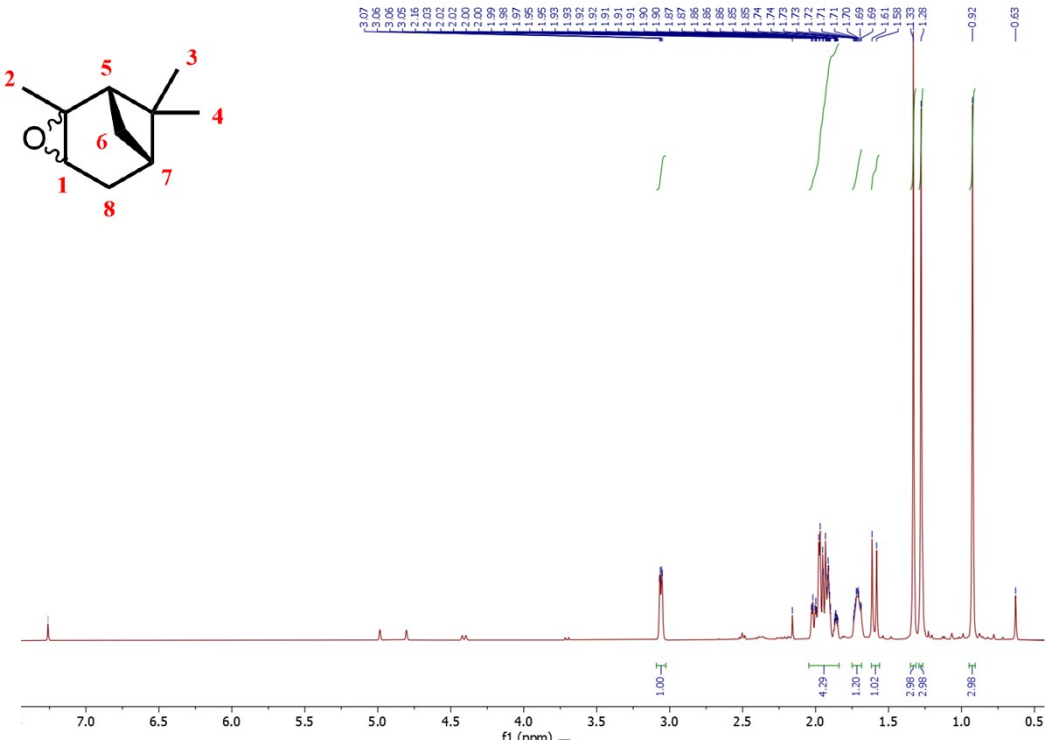

Figure S24. 1H NMR spectrum of pinene oxide.

Pinene oxide: ^{1}H NMR ($CDCl_3$, 300 MHz) δ 0.93 (s, 3H, H-4, CH_3), 1.28 (s, 3H, H-3, CH_3), 1.33 (s, 3H, H-2, CH_3), 1.62 (d, 2H, CH_2, H-8, J = 9.2 Hz), 1.68-1.74 (m, 1H, CH, H-7), 1.85-2.03 (m, 5H, CH_2, CH_2, CH correlate to H-8, H-6, H-5, respectively), 3.04 (d, 1H, CH, H-1, J = 3.9 Hz).[23]

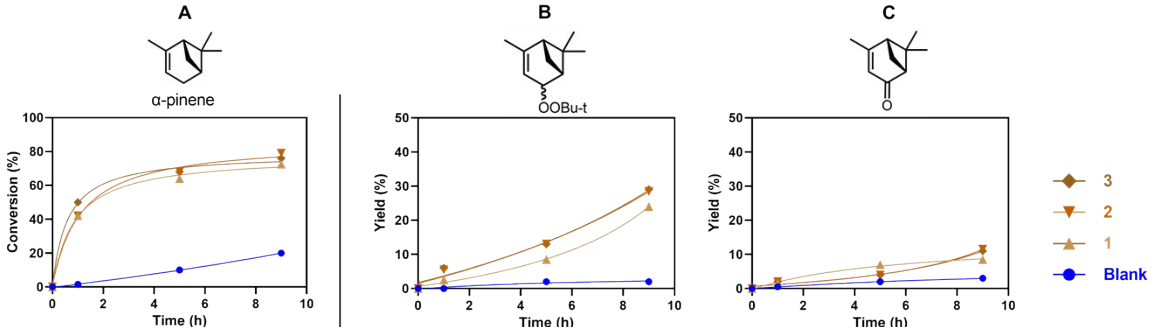

Figure S25. Oxidation of α-pinene catalyzed by different copper coordination compounds in CH_3CN at 60 ºC. Conditions: α-pinene (0.6 mmol), catalyst (**1**, **2** and **3** − 1 mol%), TBHP (70% H_2O, 1.2 mmol), CH_3CN (1 mL), 1500 rpm, 60 °C. (A: α-pinene; B: *tert*-butylperoxy-2-pinene; C: verbenone).

Table S14. Oxidation of α-pinene catalyzed by different copper coordination compounds in CH_3CN at 60 ºC.[a]

Entry	Catalyst	Amount (mol%)[b]	Conversion (%)[c]	Yield of the main products (%)[d]			
			A	**B**	**C**	**D**	**Total**
1	**1**	1.0	74.5	24.0	8.5	2.5	**35.0**
2	**2**	1.0	79.0	28.0	11.5	3.0	**42.5**
3	**3**	1.0	77.0	29.0	11.0	3.0	**43.0**
4	Blank	−	19.5	2.5	3.0	1.0	**6.5**

[a]Conditions: α-pinene (0.6 mmol), catalyst **1**, **2** and **3** − 1 mol%), TBHP (70% in H_2O; 1.2 mmol), CH_3CN (1 mL), 9 h, 1500 rpm, 60 °C. [b] *mol%*: [moles of catalyst / (moles of catalyst + moles of α-pinene) × 100]. [c] *Conversion:* [moles of α-pinene initial − moles of α-pinene final) / (moles of α-pinene) × 100]. [d] *Yield* was determined by GC based on α-pinene: (moles of product per initial mol of α-pinene) × 100. (A: α-pinene; B: *tert*-butylperoxy-2-pinene; C: verbenone; D: pinene oxide).

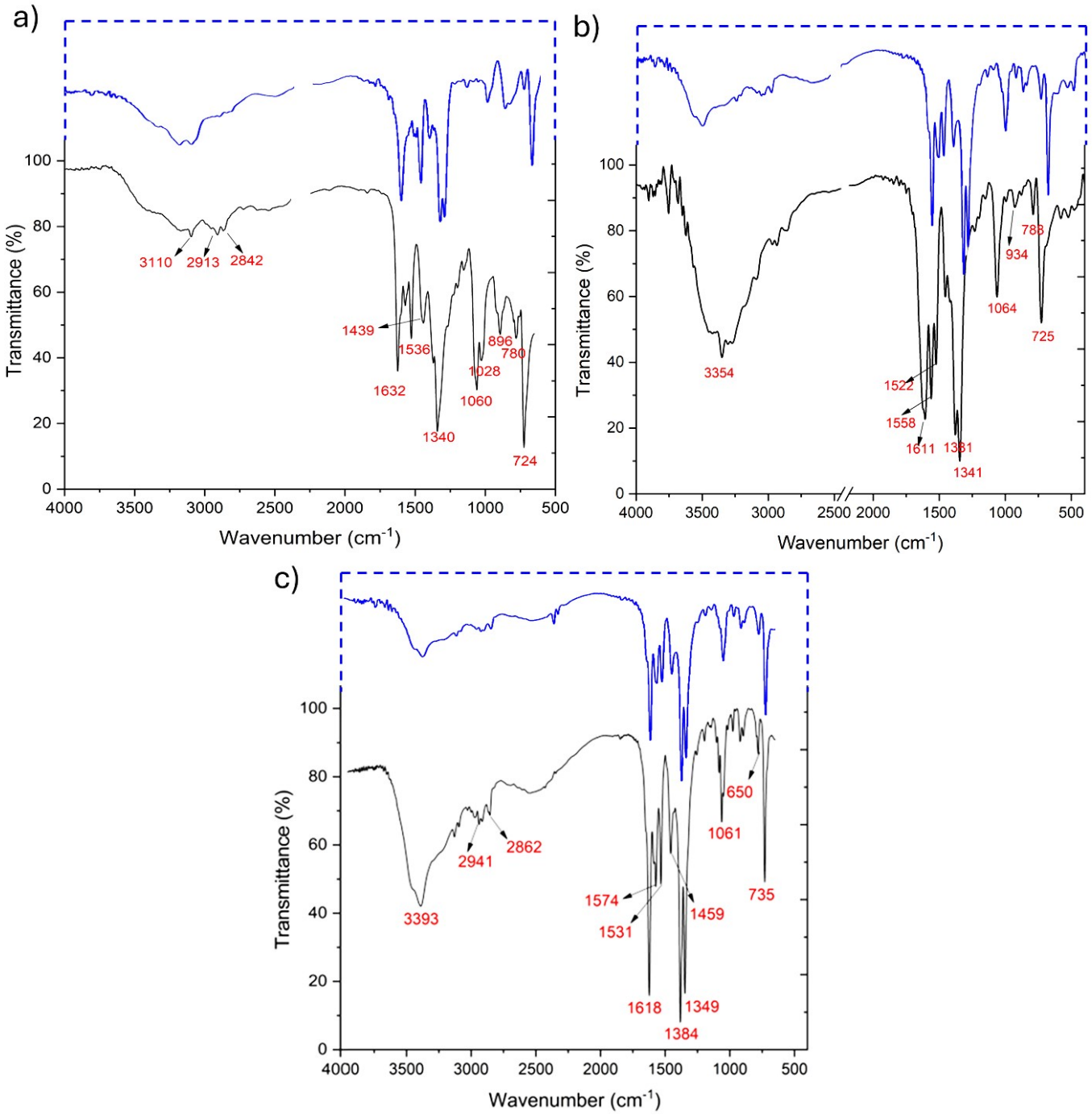

Figure S26. Infrared spectra of compounds **1** (a), **2** (b), and **3** (c): immediately obtained (black) vs. after 8 months of storage (blue).

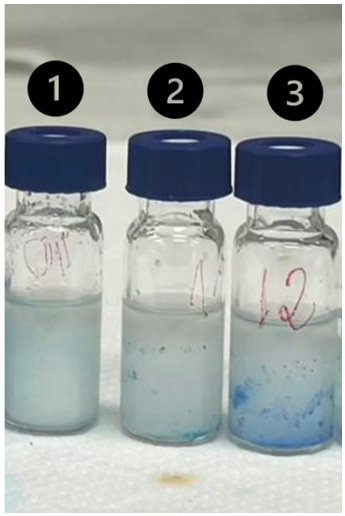

Figure S27. Solubility of 1 mol% for compounds **1**, **2**, and **3** in micellar system. Conditions: α-pinene (0.6 mmol), catalyst (0.5−2.0 mol%), TBHP (70% in H_2O, 1.2 mmol), PS-750-M (1% in H_2O, 1 mL), 6 h, 1500 rpm, 60 °C.

Supplementary references

1. https://www.chemicalbook.com/SpectrumEN_618-88-2_IR1.htm, (accessed 21/08, 2024).
2. Bruker. Apex 3, v2018. 1–0, SAINT V8. 40B. Bruker AXS Inc. Madison: 2018.
3. Sheldrick, G. *Acta Crystallogr. A*, 2015, **71**(1), 3-8.
4. O. V. Dolomanov, L. J. Bourhis, R. J. Gildea, J. A. Howard and H. Puschmann, *J. Appl. Crystallogr.*, 2009, **42**, 339-341.
5. GM, S. SHELXL-2018. Universität Göttingen: Göttingen, Germany: 2018.
6. M. A. Halcrow, *Chem. Soc. Rev.*, 2013, **42**, 1784-1795.
7. M. A. Halcrow, *Dalton Trans.*, 2003, 4375-4384.
8. J. A. de Azevedo-França, E. Barrias, C. H. J. Franco, W. Villarreal, E. G. Vieira, A. M. D. C. Ferreira, W. de Souza and M. Navarro, *J. Inorg. Biochem.*, 2022, **233**, 111834.
9. L. Schwiedrzik, V. Brieskorn and L. Gonzalez, *ACS catal.*, 2021, **11**, 13320-13329.
10. S. Hirai, S. Yagi, A. Seno, M. Fujioka, T. Ohno and T. Matsuda, *RSC adv.*, 2016, **6**, 2019-2023.
11. M. C. Etter, J. C. MacDonald and J. Bernstein, *Acta Crystallogr. B*, 1990, **46**, 256-262.
12. J. Barbier, *J. Am. Chem. Soc.*, 1997, **109**, 1056-1057.
13. V. A. Blatov, M. O'Keeffe, and D. M. Proserpio, *CrystEngComm.*, 2010, **12**, 44-48.
14. L. Yang, D. R. Powell and R. P. Houser, *Dalton Trans.*, 2007, 955-964.
15. G. Goktepeli, A. Ozgan, V. Onen, G. Ahmetli, M. Kalem and E. Yel, *Int. J. Environ. Sci. Technol.*, 2024, 1-18.
16. A. G. Blackman, E. B. Schenk, R. E. Jelley, E. H. Krenske and L. R. Gahan, *Dalton Trans.*, 2020, **49**, 14798-14806.
17. D. Sarma, K. Ramanujachary, N. Stock and S. Natarajan, *Cryst. Growth Des.*, 2011, **11**, 1357-1369.
18. L. Capaldo and D. Ravelli, *Eur. J. Org. Chem.*, 2017, **2017**, 2056-2071.
19. A. Bravo, H.-R. Bjørsvik, F. Fontana, L. Liguori and F. Minisci, *J. Org. Chem.*, 1997, **62**, 3849-3857.
20. S. Yagishita, A. Himegi, K. Kanazashi, T. Ohishi, R. Ishikawa, T. Hamaguchi and S. Kawata, *Dalton Trans.*, 2017, **46**, 2966-2973.

21. M. Schulz, R. Kluge and F. G. Gelalcha, *Tetrahedron: Asymmetry*, 1998, **9**, 4341-4360.
22. L. C. Passaro and F. X. Webster, *J. Agric. Food. Chem.*, 2004, **52**, 2896-2899.
23. J. H. Bermudez, G. Rojas, R. B. Benitez and J. M. Franco, *J. Braz. Chem. Soc.*, 2020, **31**, 1086-1092.